

# SpecSTG: A Fast Spectral Diffusion Framework for Probabilistic Spatio-Temporal Traffic Forecasting

Lequan Lin<sup>1\*†</sup>, Dai Shi<sup>1†</sup>, Andi Han<sup>2</sup> and Junbin Gao<sup>1</sup>

<sup>1</sup>The University of Sydney

<sup>2</sup>Riken AIP

{lequan.lin, dai.shi, junbin.gao}@sydney.edu.au, andi.han@riken.jp

## Abstract

Traffic forecasting, a crucial application of spatio-temporal graph (STG) learning, has traditionally relied on deterministic models for accurate point estimations. Yet, these models fall short of identifying latent risks of unexpected volatility in future observations. To address this gap, probabilistic methods, especially variants of diffusion models, have emerged as uncertainty-aware solutions. However, existing diffusion methods typically focus on generating separate future time series for individual sensors in the traffic network, resulting in insufficient involvement of spatial network characteristics in the probabilistic learning process. To better leverage spatial dependencies and systematic patterns inherent in traffic data, we propose SpecSTG, a novel spectral diffusion framework. Our method generates the Fourier representation of future time series, transforming the learning process into the spectral domain enriched with spatial information. Additionally, our approach incorporates a fast spectral graph convolution designed for Fourier input, alleviating the computational burden associated with existing models. Numerical experiments show that SpecSTG achieves outstanding performance with traffic flow and traffic speed datasets compared to state-of-the-art baselines. The source code for SpecSTG is available at <https://anonymous.4open.science/r/SpecSTG>.

## 1 Introduction

Traffic forecasting on road networks is an essential application domain of spatio-temporal graph (STG) learning [Yuan and Li, 2021; Jin *et al.*, 2023a; Jin *et al.*, 2023b]. As a crucial component of the Intelligence Transportation System (ITS), accurate and informative prediction of future traffic dynamics provides essential guidelines to traffic authorities in decision-making [Lana *et al.*, 2018; Boukerche *et al.*, 2020]. Since traffic data, such as vehicle speed and traffic flow, are

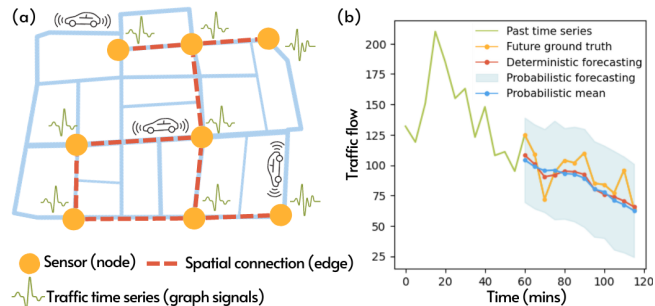


Figure 1: Illustrations: (a) an example of traffic STG; (b) traffic flow forecasting in future 60 minutes with GMAN (deterministic) and SpecSTG (probabilistic) on PEMS04.

collected from sensors in the continuous space of road networks, they present strong spatio-temporal dependencies, especially at neighbouring locations and time windows [Guo *et al.*, 2019]. This naturally leads to their representation as STGs: the traffic network is modelled as a graph, in which nodes are sensors and edges are decided with some criteria such as geographic distances. Hence, temporal records are stored as graph signals, while spatial information is encapsulated in the graph structure. In Figure 1 (a), we provide a visualized example of traffic STG.

STG traffic forecasting aims at predicting the future values at all sensors given past time series as conditions with the assistance of spatial information. This task has traditionally relied on deterministic models such as DCRNN [Li *et al.*, 2018] and GMAN [Zheng *et al.*, 2020] to produce accurate point estimations on the central tendency of future time series. Nevertheless, these models fall short in identifying the latent risk of uncertainties in temporal data, especially some unexpected variations that lead to consequential change in traffic regulations [Pal *et al.*, 2021; Wen *et al.*, 2023; Hu *et al.*, 2023]. This limitation can be overcome by probabilistic methods, which alternatively approximate the distribution of future time series, and then make uncertainty-aware predictions by sampling from the learned distribution. In Figure 1 (b), we compare the outcomes of deterministic and probabilistic models on the PEMS04 traffic flow forecasting task [Guo *et al.*, 2019]. While both models capture the decreasing trend, the probabilistic model is apparently more informative with accurate predictions of future variations.

\*The corresponding author.

†Equal contributions.

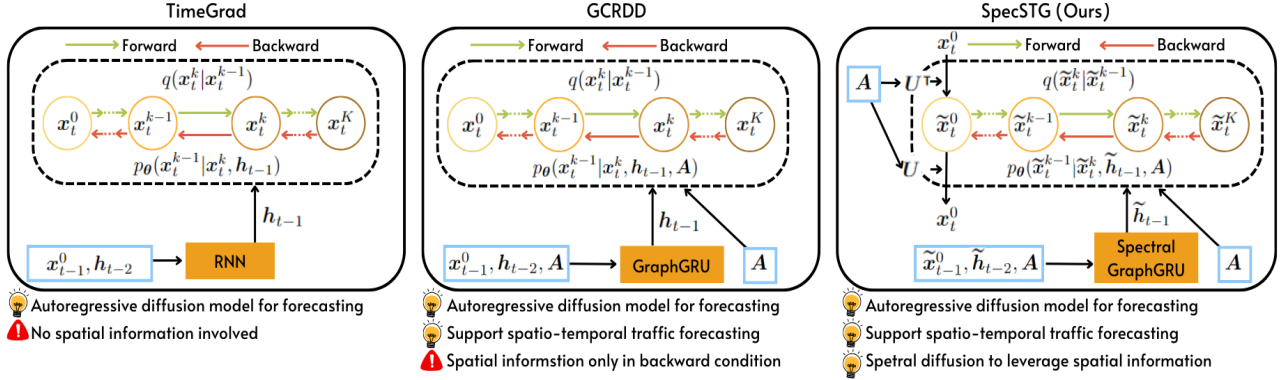


Figure 2: The overview of SpecSTG. Illustrations of TimeGrad and GCRDD are provided to show the novelty and advantage of our approach.

Among all the probabilistic models applicable to STG traffic forecasting, we specifically focus on diffusion models [Yang *et al.*, 2023; Croitoru *et al.*, 2023]. Unless otherwise stated, diffusion models mentioned in this paper are all variants of denoising diffusion probabilistic models (DDPMs), a classic formulation of score-based generative diffusion models [Sohl-Dickstein *et al.*, 2015; Ho *et al.*, 2020]. Diffusion models are more flexible with distribution assumptions compared to other probabilistic approaches. Additionally, they have demonstrated very promising performance in versatile time series and graph tasks [Lin *et al.*, 2023; Fan *et al.*, 2023]. Existing diffusion models for STG forecasting, such as DiffSTG [Wen *et al.*, 2023] and GCRDD [Li *et al.*, 2023], generally follow a forward-backward training process: they first turn the generative target (i.e., future time series) into white noises through multiple noise injection steps, and then learn a backward kernel (i.e., a conditional distribution) using the noised data, past time series, and graph structure as conditions to recover the original data in the same number of steps. Eventually, samples from the target distribution of future time series are generated by denoising random white noises with the learned backward kernel.

There are two limitations of existing diffusion methods: (1) their generative targets are separate future time series of each individual sensor that contains only temporal information, resulting in limited usage of graph structure in the forward and backward paths; (2) the substantial reliance on graph convolution to approximate the backward kernel as a denoising neural network generally causes slow training and sampling, especially with large traffic networks. To address these issues, we propose a novel spectral diffusion framework (SpecSTG), which adopts graph Fourier representation of time series as the generative target (See Figure 2 for an overview of our method and comparison with some existing works). Taking time points as features, one may apply the Fourier transform to obtain coefficients at all sensors in the spectral domain, which are measurements of different frequency components in the simultaneous records across the entire traffic network guided by the graph structure [Chung, 1997; Kreuzer *et al.*, 2021]. The Fourier representation composed of these coefficients at all times forms new spatial-involved

time series of global variations in the network. So, the first limitation is solved by generating the Fourier representation rather than the original time series, transforming the diffusion learning process to the spectral domain enriched by spatial information. This way effectively leverages the graph structure to construct a more comprehensive forecasting base with additional systematic trends and patterns. Besides, with no loss of temporal information, the generated data can be converted back to the original domain via the inverse Fourier transform before evaluation. The second limitation is addressed by replacing graph convolution with a light-complexity alternative, designed especially for Fourier input, which will be discussed in detail in Section 4.3.

The contributions of this paper are threefold:

- (1) To our best knowledge, this is a pioneering work that explores the efficacy of probabilistic STG forecasting on the graph spectral domain;
- (2) Our method establishes a comprehensive probabilistic forecasting base that incorporates both spatial and temporal patterns with a special focus on the traffic application domain;
- (3) Numerical experiments show that our method is competitive with state-of-the-art diffusion baselines and is computationally efficient in training and sampling.

## 2 Related Works

**Diffusion models for STG forecasting** Pioneering diffusion models for time series such as TimeGrad [Rasul *et al.*, 2021a] and CSDI [Tashiro *et al.*, 2021] were originally tailored for multivariate time series forecasting, utilizing sensors as variables but only exploring general dependencies without incorporating graph structural information. Recently, several diffusion models were proposed specifically for STG forecasting. DiffSTG [Wen *et al.*, 2023] incorporates graph structure into the backward kernel with a graph-modified Unet [Ronneberger *et al.*, 2015] architecture. GCRDD [Li *et al.*, 2023], designed in reminiscent of TimeGrad, adopts a graph-enhanced recurrent encoder to produce hidden states from past time series as conditions. Additionally, USTD [Hu *et al.*, 2023] introduces a pre-trained encoder that better

captures deterministic patterns via an unsupervised reconstruction task. DVGNN [Liang *et al.*, 2023] is a deterministic model but with a diffusion module to generate dynamic adjacency matrices in its pre-training process. Furthermore, PriSTI [Liu *et al.*, 2023] was initially developed from CSDI [Tashiro *et al.*, 2021] for STG imputation, but with potential for forecasting tasks by masking future data as missing values. SpecSTG’s novelty lies in its incorporation of spatial dependencies in the generative target rather than simply focusing on temporal tendencies.

**Spectral diffusion on graphs** The idea of spectral diffusion has also been applied in graph generation. Different from SpecSTG whose focus is on generating spectral temporal graph signals, GSMD [Luo *et al.*, 2023] explores the generation of spectral graph structure, i.e., the eigenvalues of graph adjacency matrices, to enhance graph synthesis quality.

### 3 Preliminaries

#### 3.1 Spatio-Temporal Graphs

STGs can be considered as a multidimensional graph representation of entities in a system with time series as graph signals. In traffic forecasting, we model sensors as nodes and then create edges based on some spatial relationships such as geographic distances. The average traffic records in observation periods are modelled as graph signals. For a traffic network with  $N$  sensors, the corresponding STG can be denoted as  $\mathcal{G}\{\mathcal{V}, \mathcal{E}, \mathbf{A}\}$ , where  $\mathcal{V}$  is the set of nodes/sensors,  $\mathcal{E}$  is the set of edges, and  $\mathbf{A} \in \mathbb{R}^{N \times N}$  is the adjacency matrix.  $\mathbf{A}$  is assumed to be undirected and can be either weighted or unweighted. The graph signals are denoted as  $\mathbf{X}_{\mathcal{G}} = \{\mathbf{x}_1, \mathbf{x}_2, \dots, \mathbf{x}_t, \dots | \mathbf{x}_t \in \mathbb{R}^{N \times D_x}\}$ , where  $D_x$  is the number of variables. In traffic forecasting, it is common that only one variable such as speed or flow is of interest [Li *et al.*, 2018; Guo *et al.*, 2019], thus we have  $D_x = 1$  such that  $\mathbf{x}_t \in \mathbb{R}^N$ .

#### 3.2 Problem Formulation

The objective of STG traffic forecasting is to predict a future time series window  $\mathbf{X}_f = \{\mathbf{x}_{t_0+1}, \mathbf{x}_{t_0+2}, \dots, \mathbf{x}_{t_0+f}\}$  given the past context window  $\mathbf{X}_c = \{\mathbf{x}_{t_0-c+1}, \mathbf{x}_{t_0-c+2}, \dots, \mathbf{x}_{t_0}\}$ , where  $f$  and  $c$  are the length of future and past windows. We denote  $\mathbf{X} = \{\mathbf{x}_{t_0-c+1}, \mathbf{x}_{t_0-c+2}, \dots, \mathbf{x}_{t_0+f}\}$  as the combination of past and future time series. Normally, the target distribution of generative models depends on the sampling methods: one-shot methods produce all future predictions together from the distribution  $q(\mathbf{X}_f | \mathbf{X}_c, \mathbf{A})$  [Wen *et al.*, 2023; Liu *et al.*, 2023], while autoregressive methods generate samples from  $q(\mathbf{x}_t | \mathbf{X}_{t_0-c+1:t-1}, \mathbf{A})$  for  $t = t_0 + 1, t_0 + 2, \dots, t_0 + f$  successively, where  $\mathbf{X}_{t_0-c+1:t-1} = \{\mathbf{x}_{t_0-c+1}, \dots, \mathbf{x}_{t-1}\}$  [Li *et al.*, 2023]. Autoregressive methods often capture the sequential information in consecutive time points more closely. However, they are associated with higher time costs because of the non-parallel step-by-step sampling process. Our method, SpecSTG, is formulated within the autoregressive framework but is equipped with a specially designed spectral graph convolution to mitigate computational inefficiency.

### 4 Methodology

#### 4.1 Spatio-Temporal Graph Fourier Transform

Given a traffic STG  $\mathcal{G}\{\mathcal{V}, \mathcal{E}, \mathbf{A}\}$  with  $N$  sensors, the normalized graph Laplacian is computed as  $\mathbf{L} = \mathbf{I}_N - \mathbf{D}^{-\frac{1}{2}} \mathbf{A} \mathbf{D}^{-\frac{1}{2}}$ , where  $\mathbf{I}_N \in \mathbb{R}^{N \times N}$  is the identity matrix, and  $\mathbf{D} \in \mathbb{R}^{N \times N}$  is the diagonal degree matrix. We denote the eigen-decomposition of the graph Laplacian as  $\mathbf{L} = \mathbf{U} \Lambda \mathbf{U}^\top$ , where  $\mathbf{U} \in \mathbb{R}^{N \times N}$  and  $\Lambda \in \mathbb{R}^{N \times N}$  are the corresponding eigenvector and eigenvalue matrices, respectively. Considering the univariate graph signal  $\mathbf{X}_{\mathcal{G}} = \{\mathbf{x}_1, \mathbf{x}_2, \dots, \mathbf{x}_t, \dots | \mathbf{x}_t \in \mathbb{R}^N\}$ , the Fourier transform for each time point  $t$  is given by  $\tilde{\mathbf{x}}_t = \mathbf{U}^\top \mathbf{x}_t$ , known as the Fourier representation of  $\mathbf{x}_t$  in the spectral domain. The Fourier reconstruction is  $\mathbf{x}_t = \mathbf{U} \tilde{\mathbf{x}}_t$ . The orthonormal  $\mathbf{U}$  ensures a lossless reconstruction for the temporal information. We may compute in matrix form for all time points as  $\tilde{\mathbf{X}} = \mathbf{U}^\top \mathbf{X}$  and  $\mathbf{X} = \mathbf{U} \tilde{\mathbf{X}}$ . In **Appendix A**, we also discuss how to naturally extend the method to multivariate traffic STGs with  $\mathbf{x}_t \in \mathbb{R}^{N \times D_x}$ ,  $D_x \geq 2$ .

The graph Fourier transform can be understood as a projection of graph signals onto the spectral domain spanned by the eigenvector basis of graph Laplacian. The operator  $\mathbf{U}$  brings rich positional information for graph signals and offers a platform to investigate the variations among signals through a global perspective on the graph. In particular, when the input is a traffic STG, the Fourier representation measures how graph signals (time series values) fluctuate across the network. This effectively integrates spatial connectivity into time series, leading to a spatial-aware forecasting paradigm.

#### 4.2 Denoising Diffusion Probabilistic Model

Denoising diffusion probabilistic models (DDPMs) learn how to generate samples from the target distribution via a pair of forward-backward Markov chains [Ho *et al.*, 2020; Yang *et al.*, 2023]. Assuming that  $\mathbf{x}^0 \sim q(\mathbf{x}^0)$  is the original data, for diffusion step  $k = 0, 1, \dots, K$ , the forward chain injects Gaussian noises to  $\mathbf{x}^k$  until  $q(\mathbf{x}^K) := \int q(\mathbf{x}^K | \mathbf{x}^0) q(\mathbf{x}^0) d\mathbf{x}^0 \approx \mathcal{N}(\mathbf{x}^K; \mathbf{0}, \mathbf{I})$ . As a special property, given a noise schedule  $\beta = \{\beta_1, \beta_2, \dots, \beta_K\}$ , we may directly compute the disturbed data at step  $k$  as  $\mathbf{x}^k = \sqrt{\tilde{\alpha}_k} \mathbf{x}^0 + \sqrt{1 - \tilde{\alpha}_k} \boldsymbol{\epsilon}$ , where  $\tilde{\alpha}_k = \prod_{i=1}^k (1 - \beta_i)$  and  $\boldsymbol{\epsilon} \sim \mathcal{N}(\mathbf{0}, \mathbf{I})$ . Next, the backward chain denoises from  $\mathbf{x}^K$  to recover  $p_{\theta}(\mathbf{x}^0)$  through a probabilistic backward kernel  $p_{\theta}(\mathbf{x}^{k-1} | \mathbf{x}^k)$ , where  $\theta$  denotes all learnable parameters. In practice, the backward kernel is usually optimized with a denoising network  $\epsilon_{\theta}$  by minimizing the loss function

$$\mathcal{L}_{DDPM}(\theta) = \mathbb{E}_{k, \mathbf{x}^0, \boldsymbol{\epsilon}} \|\boldsymbol{\epsilon} - \epsilon_{\theta}(\mathbf{x}^k, k)\|^2, \quad (1)$$

where  $\boldsymbol{\epsilon} \sim \mathcal{N}(\mathbf{0}, \mathbf{I})$  represents the noises injected in the forward diffusion steps. Please refer to **Appendix B** for more details on DDPMs.

#### 4.3 SpecSTG Architecture

##### Overview

SpecSTG assumes that the Fourier representation of future time series follows the distribution

$$q(\tilde{\mathbf{X}}_f^0 | \tilde{\mathbf{X}}_c^0, \mathbf{A}) \approx \prod_{t=t_0+1}^{t_0+f} p_{\theta}(\tilde{\mathbf{x}}_t^0 | \tilde{\mathbf{h}}_{t-1}, \mathbf{A}), \quad (2)$$

where  $\tilde{\mathbf{X}}_c^0$  and  $\tilde{\mathbf{X}}_f^0$  are the noise-free Fourier representations of past and future time series, respectively.  $\tilde{\mathbf{h}}_{t-1} = \text{SG-GRU}_\theta(\tilde{\mathbf{x}}_{t-1}^0, \tilde{\mathbf{h}}_{t-2}, \mathbf{A})$  is the hidden state computed with Spectral Graph Gated Recurrent Units (SG-GRU), which is a recurrent module adapted to Fourier input to better encode past temporal dynamics following the idea in [Seo *et al.*, 2018]. For each time point  $t = t_0 + 1, \dots, t_0 + f$ , the diffusion process will learn the corresponding backward kernel  $p_\theta(\tilde{\mathbf{x}}_t^{k-1} | \tilde{\mathbf{x}}_t^k, \tilde{\mathbf{h}}_{t-1}, \mathbf{A})$  with  $k = 1, \dots, K$ . Under Equation (7), the objective function of SpecSTG is given by

$$\mathcal{L}(\theta) = \mathbb{E}_{t,k,\tilde{\mathbf{x}}_t^0, \epsilon_t} \left\| \epsilon_t - \epsilon_\theta(\tilde{\mathbf{x}}_t^k, k, \tilde{\mathbf{h}}_{t-1}, \mathbf{A}) \right\|^2, \quad (3)$$

where  $t$  denotes future time points,  $k$  denotes diffusion steps,  $\tilde{\mathbf{x}}_t^k$  is the disturbed data at time point  $t$  and step  $k$ , and  $\epsilon_t \sim \mathcal{N}(\mathbf{0}, \mathbf{I})$ . It is worth noting that  $t$  may also start with  $t_0 - c + 1$  instead of  $t_0 + 1$  to facilitate the learning of autoregressive dependencies by considering both past and future instances. Lastly, taking the idea from DiffWave [Kong *et al.*, 2021] and TimeGrad [Rasul *et al.*, 2021a], we employ a graph-modified WaveNet architecture [van den Oord *et al.*, 2016a] for  $\epsilon_\theta(\cdot)$ , which is also designed for Fourier input. Details of SpecSTG components are discussed in the rest of this section, and the visualized overview of SpecSTG can be found in Figure 2.

### Spectral Graph Convolution

Diffusion models for STG forecasting usually rely on graph convolution to encode spatial information in the condition of backward kernel [Li *et al.*, 2023; Wen *et al.*, 2023; Liu *et al.*, 2023]. Straightforwardly, we adopt the spectral convolution, which typically transforms graph signals to the spectral domain and then processes the data via frequency filtering before they are converted back to the original domain [Defferrard *et al.*, 2016; Kipf and Welling, 2016]. However, with SpecSTG, the Fourier representation is already formed as input, so the transform is no longer required in the convolution. In addition, to ensure that the model pipeline flows in the spectral domain throughout the diffusion learning process, we do not apply reconstruction either.

We choose the Chebyshev convolution [Defferrard *et al.*, 2016], whose filters are formed with Chebyshev polynomials to accelerate computation as  $\text{ChebConv}(\mathbf{X}) = \mathbf{U} \sum_{j=0}^{J-1} \phi_j \mathcal{T}_j(\tilde{\Lambda}) \mathbf{U}^\top \mathbf{X}$ , for polynomial degrees up to  $J-1$ , where  $\mathcal{T}_j(\tilde{\Lambda}) \in \mathbb{R}^{N \times N}$  is the  $j$ -th order Chebyshev polynomial evaluated at  $\tilde{\Lambda} = 2\Lambda/\lambda_{\max} - \mathbf{I}_N$  with  $\phi_j$  being a learnable coefficient. With Fourier representation  $\tilde{\mathbf{X}} = \mathbf{U}^\top \mathbf{X}$  as input, we define the modified spectral graph convolution as

$$\text{SpecConv}(\tilde{\mathbf{X}}) := \sum_{j=0}^{J-1} \phi_j \mathcal{T}_j(\tilde{\Lambda}) \tilde{\mathbf{X}}. \quad (4)$$

*Remark 1* (Complexity Analysis). Our spectral convolution has only  $\mathcal{O}(N)$  complexity, contrasting to the  $\mathcal{O}(N^2)$  complexity of the classic Chebyshev convolution. This significant improvement endows SpecSTG with the advantage of time efficiency over methods using Chebyshev convolution, such as GCRDD. Other methods such as DiffSTG may

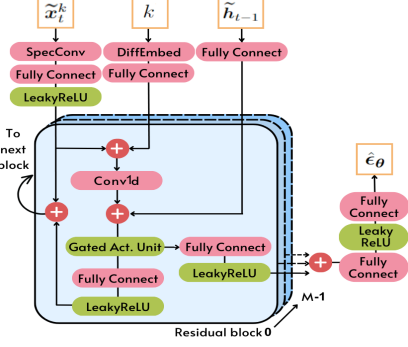


Figure 3: The denoising network  $\epsilon_\theta$ : a modified WaveNet structure.

use the graph convolution in [Kipf and Welling, 2016] as  $\text{GCNConv}(\mathbf{X}) = \mathbf{A}\mathbf{X}$ , whose complexity is  $\mathcal{O}(|\mathcal{E}|)$  where  $|\mathcal{E}|$  is the number of edges. As we see in Section 5.1,  $|\mathcal{E}|$  is often much larger than  $N$  in traffic STGs.

### Spectral Graph Gated Recurrent Units

Enlightened by the idea in [Seo *et al.*, 2018], we design SG-GRU to encode past time series enriched with spatial information as follows. For  $t = t_0 - c + 1, \dots, t_0$ :

$$\begin{aligned} z &= \sigma(\text{SpecConv}(\tilde{\mathbf{x}}_t^0) \mathbf{W}_{z_1} + \text{SpecConv}(\tilde{\mathbf{h}}_{t-1}) \mathbf{W}_{z_2}) \\ r &= \sigma(\text{SpecConv}(\tilde{\mathbf{x}}_t^0) \mathbf{W}_{r_1} + \text{SpecConv}(\tilde{\mathbf{h}}_{t-1}) \mathbf{W}_{r_2}) \\ \zeta &= \tanh(\text{SpecConv}(\tilde{\mathbf{x}}_t^0) \mathbf{W}_{\zeta_1} + \text{SpecConv}(\mathbf{r} \odot \tilde{\mathbf{h}}_t) \mathbf{W}_{\zeta_2}) \\ \tilde{\mathbf{h}}_{t+1} &= \mathbf{z} \odot \tilde{\mathbf{h}}_t + (1 - \mathbf{z}) \odot \zeta, \end{aligned}$$

where  $\tilde{\mathbf{h}}_0 \in \mathbb{R}^{D_h}$  is a vector of zeros with  $D_h$  being the hidden size,  $\mathbf{W}_{z_1}, \mathbf{W}_{r_1}, \mathbf{W}_{\zeta_1} \in \mathbb{R}^{1 \times D_h}$ ,  $\mathbf{W}_{z_2}, \mathbf{W}_{r_2}, \mathbf{W}_{\zeta_2} \in \mathbb{R}^{D_h \times D_h}$  are learnable weights included in  $\theta$ , and  $\sigma$  is the sigmoid activation function.  $\mathbf{z}$  and  $\mathbf{r}$  are known as update gate and reset gate.  $\zeta$  is the candidate state storing current information to be updated in the hidden state. In the implementation, we may also input time features  $\Gamma = \{\gamma_{t_0-c+1}, \gamma_{t_0-c+2}, \dots, \gamma_{t_0+f}\}$  such as day of week and week of month by concatenating them with  $\tilde{\mathbf{X}}$ .

### Denoising Network

In reminiscent of DiffWave and TimeGrad, we design Spectral Graph WaveNet (SG-Wave) as the  $\epsilon_\theta$  of SpecSTG (Figure 3). Besides, following the implementation of GCRDD, we replace some Conv1d layers with fully connected linear layers for efficient training and sampling. The network takes disturbed data  $\tilde{\mathbf{x}}_t^k$ , diffusion step  $k$ , hidden condition  $\tilde{\mathbf{h}}_{t-1}$ , and graph adjacency  $\mathbf{A}$  as inputs, and aims at predicting the noise  $\epsilon_t \sim \mathcal{N}(\mathbf{0}, \mathbf{I})$  at step  $k$  for time point  $t$ . For  $m = 0, \dots, M-1$ , we compute multiple residual blocks recursively as

$$\begin{aligned} \rho_m &= \text{LeakyReLU}(\text{SpecConv}(\tilde{\mathbf{x}}_{t,m}^k) \mathbf{W}_x) \\ \delta_m &= \text{Conv1d}(\rho_m + \text{DiffEmbed}(k) \mathbf{W}_k) \\ \mathbf{g}_m &= \text{GatedActivationUnit}(\delta_m + \tilde{\mathbf{h}}_{t-1} \mathbf{W}_h) \\ \tilde{\mathbf{x}}_{t,m+1}^k &= \tilde{\mathbf{x}}_{t,m}^k + \text{LeakyReLU}(\mathbf{g}_m \mathbf{W}_{g_1}), \\ \mathbf{g}_{m+1} &= \text{LeakyReLU}(\mathbf{g}_m \mathbf{W}_{g_2}) \end{aligned}$$

---

**Algorithm 1** SpecSTG training

---

**Input:** The distribution of training data after Fourier transform:  $q(\{\tilde{\mathbf{X}}_c, \tilde{\mathbf{X}}_f\})$ ; hidden states:  $\tilde{\mathbf{h}}$ ; number of diffusion steps:  $K$ ; noise schedule  $\{\beta_1, \beta_2, \dots, \beta_K\}$ , graph:  $\mathcal{G}(\mathcal{V}, \mathcal{E}, \mathbf{A})$ .

**Output:** Optimized denoising network  $\epsilon_{\theta}$ .

```

1: Sample  $\{\tilde{\mathbf{X}}_c, \tilde{\mathbf{X}}_f\} \sim q(\{\tilde{\mathbf{X}}_c, \tilde{\mathbf{X}}_f\})$ 
2: while Not Convergence do
3:   for  $t = t_0 + 1, t_0 + 2, \dots, t_0 + f$  do
4:      $k \sim \text{Uniform}(1, K)$ ,  $\epsilon_t \sim \mathcal{N}(\mathbf{0}, \mathbf{I})$ 
5:     Compute  $\tilde{\mathbf{x}}_t^k = \sqrt{\tilde{\alpha}_k} \tilde{\mathbf{x}}_t^0 + \sqrt{1 - \tilde{\alpha}_k} \epsilon_t$ 
6:   end for
7:   Take gradient step on and do gradient descent for  $\theta$ 
     $\nabla_{\theta} \mathbb{E}_{t,k,\tilde{\mathbf{x}}_t^0, \epsilon_t} \left\| \epsilon_t - \epsilon_{\theta} \left( \tilde{\mathbf{x}}_t^k, k, \tilde{\mathbf{h}}_{t-1}, \mathbf{A} \right) \right\|^2$ 
8: end while

```

---

where  $\tilde{\mathbf{x}}_{t,0}^k = \tilde{\mathbf{x}}_t^k$ , DiffEmbed( $\cdot$ ) is the embedding of diffusion steps, and GatedActivationUnit( $\cdot$ ) =  $\sigma(\cdot) \odot \tanh(\cdot)$  is from [Van den Oord *et al.*, 2016b]. Eventually, the network predicts as

$$\hat{\epsilon}_{\theta} = \text{LeakyReLU} \left( \sum_{m=0}^{M-1} \eta_{m+1} \mathbf{W}_{\epsilon_1} \right) \mathbf{W}_{\epsilon_2}. \quad (5)$$

$\mathbf{W}_x \in \mathbb{R}^{1 \times D_r}$ ,  $\mathbf{W}_k, \mathbf{W}_h \in \mathbb{R}^{D_h \times D_r}$ ,  $\mathbf{W}_{g_2}, \mathbf{W}_{\epsilon_1} \in \mathbb{R}^{D_r \times D_r}$ ,  $\mathbf{W}_{g_1}, \mathbf{W}_{\epsilon_2} \in \mathbb{R}^{D_r \times 1}$  are all learnable weights contained in  $\theta$ , where  $D_r$  is the number of residual channels.

#### 4.4 Training and Inference

We compute the Fourier representation of all training data before the training process. Next, we input randomly sampled  $\{\tilde{\mathbf{X}}_c, \tilde{\mathbf{X}}_f\}$  to SG-GRU $_{\theta}$  to obtain hidden states  $\tilde{\mathbf{h}} = \{\tilde{\mathbf{h}}_{t_0}, \dots, \tilde{\mathbf{h}}_{t_0+f-1}\}$ . During training, with a pre-specified noise schedule  $\{\beta_1, \beta_2, \dots, \beta_K\}$ , we randomly sample noise  $\epsilon_t \sim \mathcal{N}(\mathbf{0}, \mathbf{I})$  and step  $k \sim \text{Uniform}(0, K)$  to compute disturbed data  $\tilde{\mathbf{x}}_t^k$  for  $t = t_0 + 1, t_0 + 2, \dots, t_0 + f$ . Finally, we take a gradient step on the objective function in Equation (3). The training algorithm is provided in Algorithm 1. With the denoising network, we can generate samples and make predictions for the forecasting task. The generation process adopts autoregressive sampling, which means we generate samples for each time point one by one. For example, after we generate samples for  $t = t_0 + 1$ , we feed the sample mean back to the SG-GRU module to compute  $\tilde{\mathbf{h}}_{t_0+1}$ , and then use it to generate samples for  $t = t_0 + 2$ . Lastly, we convert the predictions back to the original domain via Fourier reconstruction. The sampling and prediction algorithm for a one-time point  $x_t^0$  is presented in Algorithm 2.

## 5 Experiments

### 5.1 Datasets and Baseline Models

We validate our model on two traffic datasets, PEMS04 and PEMS08 [Guo *et al.*, 2019], collected by the California

---

**Algorithm 2** SpecSTG sampling and prediction for  $x_t^0$ 


---

**Input:** Hidden state:  $\tilde{\mathbf{h}}_{t-1}$ ; Fourier operator  $\mathbf{U}$ ; number of samples:  $S$ ; variance hyperparameter:  $\sigma_k$ .

**Output:** Prediction  $\hat{x}_t^0$ .

```

1: Randomly generate  $S$  samples  $\{\tilde{\mathbf{x}}_{t,s}^K\}_{s=1}^S \sim \mathcal{N}(\mathbf{0}, \mathbf{I})$  and
   do the follows in parallel for all  $s$ .
2: for  $k = K, K-1, \dots, 1$  do
3:    $e = \mathbf{0}$  if  $k = 1$  else  $e \sim \mathcal{N}(\mathbf{0}, \mathbf{I})$ 
4:   Compute and update  $\tilde{\mathbf{x}}_{t,s}^{k-1}$  as
    
$$\frac{1}{\sqrt{1-\beta_k}} \left( \tilde{\mathbf{x}}_{t,s}^k - \frac{\beta_k}{\sqrt{1-\tilde{\alpha}_k}} \epsilon_{\theta}(\tilde{\mathbf{x}}_{t,s}^k, k, \tilde{\mathbf{h}}_{t-1}, \mathbf{A}) \right) + \sigma_k e$$

5: end for
6: Take average on  $S$  samples  $\tilde{\mathbf{x}}_t^0 = \frac{1}{S} \sum_{s=1}^S \tilde{\mathbf{x}}_{t,s}^0$ 
7: Compute predictions  $\hat{\mathbf{x}}_t^0 = \mathbf{U} \tilde{\mathbf{x}}_t^0$ 

```

---

Transportation Agencies’ (CalTrans) Performance Measurement System (PEMS) [Chen *et al.*, 2001]. PEMS04 comprises traffic records from 307 sensors in California’s District 04 from Jan 1st to Feb 28th, 2018, while PEMS08 includes data from 170 sensors in District 08 from July 1st to 31st August 2018. Our experiments focus on traffic flow and speed available in both datasets, denoted as “F” and “S” respectively. For instance, “PEMS04F” denotes traffic flow records in the PEMS04 dataset. Each time point covers 5 minutes, with the corresponding value representing the average records during that interval. The speed data are continuous, allowing us to introduce random Gaussian noises. Although traffic flow (i.e., the number of vehicles) is a discrete variable, we still treat it as continuous considering the fact that it contains numerous unique values. More details about the datasets can be found in Table 1.

Five probabilistic baselines are considered in our experiments, including two methods for classic multivariate time series forecasting: TimeGrad [Rasul *et al.*, 2021a], CSDI [Tashiro *et al.*, 2021]; and three methods for spatio-temporal forecasting: GCRDD [Li *et al.*, 2023], DiffSTG [Wen *et al.*, 2023], PriSTI [Liu *et al.*, 2023]. All baselines are state-of-the-art diffusion models proposed in recent years. We do not include USTD [Hu *et al.*, 2023] and DVGN [Liang *et al.*, 2023] as baselines because their pre-training process may lead to unfair comparison. For more discussions on the baseline models, please see **Appendix C**.

Dataset	Type	#Nodes	#Edges	#Time points
PEMS04F	Flow			
PEMS04S	Speed	307	680	16992
PEMS08F	Flow			
PEMS08S	Speed	170	548	17856

Table 1: Dataset details

Models	RMSE				MAE				CRPS			
	Avg.	15min	30min	60min	Avg.	15min	30min	60min	Avg.	15min	30min	60min
PEMS04F												
TimeGrad	35.58	33.22	35.24	38.95	21.70	20.26	21.56	24.04	0.0801	0.0747	0.0795	0.0887
CSDI	34.42	<u>31.49</u>	33.99	38.49	22.19	20.25	22.04	25.21	0.0783	0.0715	0.0777	0.0890
GCRDD	36.28	31.94	45.31	41.99	22.16	<u>19.48</u>	21.87	26.18	0.0779	<u>0.0683</u>	0.0768	0.0982
DiffSTG	37.62	34.99	36.68	43.04	24.90	22.53	24.65	29.24	0.0904	0.0815	0.0894	0.1077
PriSTI	<u>33.74</u>	33.56	<u>33.71</u>	<u>37.31</u>	22.46	21.65	22.32	25.19	<u>0.0772</u>	0.0751	<u>0.0764</u>	<b>0.0870</b>
SpecSTG	<b>33.15</b>	<b>30.07</b>	<b>32.81</b>	<b>37.29</b>	<b>21.53</b>	<b>19.29</b>	<b>21.39</b>	<b>23.29</b>	<b>0.0766</b>	<b>0.0689</b>	<b>0.0761</b>	0.0886
PEMS08F												
TimeGrad	33.09	30.17	32.53	37.51	20.47	18.24	20.06	24.24	0.0705	0.0618	0.0695	0.0843
CSDI	<u>26.13</u>	<u>23.49</u>	<u>26.05</u>	<b>29.68</b>	<b>16.82</b>	<u>15.20</u>	<u>16.84</u>	<b>19.34</b>	<b>0.0567</b>	<u>0.0509</u>	<u>0.0566</u>	<b>0.0655</b>
GCRDD	28.83	23.91	28.10	35.68	18.72	15.52	18.35	23.99	0.0626	0.0517	0.0617	0.0833
DiffSTG	28.26	25.04	27.54	34.32	18.99	16.66	18.63	23.68	0.0692	0.0609	0.0679	0.0872
PriSTI	26.35	24.58	26.93	29.91	17.30	15.98	17.32	20.67	0.0576	0.0539	0.0581	0.0688
SpecSTG	<b>25.59</b>	<b>22.23</b>	<b>24.77</b>	29.90	17.06	<b>14.93</b>	<b>16.70</b>	20.25	0.0572	<b>0.0500</b>	<b>0.0558</b>	0.0680
PEMS04S												
TimeGrad	5.92	5.62	5.91	6.35	2.38	2.19	2.37	2.66	0.0307	0.0282	0.0308	0.0345
CSDI	4.64	3.41	4.72	5.89	2.05	1.60	2.12	2.67	<u>0.0252</u>	0.0195	0.0261	<u>0.0327</u>
GCRDD	<u>4.33</u>	<u>3.10</u>	<u>4.30</u>	5.63	<u>1.94</u>	<b>1.50</b>	<b>1.97</b>	<u>2.58</u>	<b>0.0245</b>	<b>0.0189</b>	<b>0.0248</b>	0.0329
DiffSTG	4.46	3.24	4.46	5.72	2.15	1.66	2.20	2.83	0.0264	0.0206	0.0267	0.0340
PriSTI	4.42	3.31	4.67	<u>5.60</u>	1.96	1.54	<u>1.99</u>	2.62	<b>0.0245</b>	<u>0.0192</u>	<u>0.0253</u>	<b>0.0319</b>
SpecSTG	<b>4.06</b>	<b>3.01</b>	<b>4.09</b>	<b>5.15</b>	<b>1.93</b>	<u>1.52</u>	<u>1.97</u>	<b>2.51</b>	<u>0.0252</u>	0.0198	0.0258	0.0329
PEMS08S												
TimeGrad	4.98	4.93	4.97	5.03	1.98	1.95	1.97	<b>2.02</b>	0.0267	0.0262	0.0268	<b>0.0272</b>
CSDI	4.22	3.21	4.38	5.15	<u>1.69</u>	1.32	1.76	2.17	<b>0.0216</b>	<u>0.0167</u>	<u>0.0225</u>	0.0277
GCRDD	<u>3.75</u>	<u>2.74</u>	<u>3.77</u>	4.89	1.72	1.35	<u>1.75</u>	2.32	0.0223	0.0171	0.0226	0.0301
DiffSTG	3.97	3.20	4.07	<u>4.82</u>	2.36	1.91	2.43	3.04	0.0325	0.0259	0.0335	0.0423
PriSTI	4.22	3.02	4.39	<u>5.20</u>	1.70	<u>1.29</u>	1.80	2.15	<u>0.0217</u>	<b>0.0162</b>	0.0230	<u>0.0275</u>
SpecSTG	<b>3.45</b>	<b>2.58</b>	<b>3.46</b>	<b>4.36</b>	<b>1.63</b>	<b>1.27</b>	<b>1.67</b>	<u>2.12</u>	<u>0.0217</u>	0.0170	<b>0.0219</b>	0.0286

Table 2: The results of traffic forecasting experiments in a future window of 60 minutes. Average RMSE, MAE, CRPS, and their point values at 15/30/60 minutes are reported. Lower values indicate better forecasting performance. The best results are marked in **bold** and the second best results are underlined.

## 5.2 Metrics

We evaluate our model with three metrics: Root Mean Squared Error (RMSE), Mean Absolute Error (MAE), and Continuous Ranked Probability Score (CRPS). RMSE and MAE are commonly used deterministic metrics, while CRPS is a probabilistic metric that measures the compatibility of the learned probabilistic distribution with the ground truth values [Matheson and Winkler, 1976]. Please see [Appendix D](#) for calculation formulas and more explanations.

## 5.3 Implementation Details

We implement SpecSTG on a single Nvidia 4090 GPU with 64GB of memory. The model is trained with the Adam optimizer with a learning rate schedule from  $5e-4$  to  $1e-2$ . The maximum number of epochs is 300 for flow data and 50 for speed data with batch size 64. Validation loss is used for model selection. The hyperparameters specific to diffusion models are set as follows. We use the quadratic scheme for noise level  $\beta_k$  starting from  $\beta_1 = 1e-4$  and tune  $\beta_K$  in  $[0.1, 0.2, 0.3, 0.4]$ . The number of diffusion steps  $K$  is selected from  $[50, 100, 200]$ . The maximum polynomial order in SpecConv is set as 2. The hidden size  $D_h$  is tuned in  $[64, 96]$ . In SG-Wave, the number of residual blocks  $M = 8$  and the residual channel  $D_r = 8$ . Finally, the number of samples  $S$  is set as 100 for all models. For all experiments, we split datasets with 60%/20%/20% train/validation/test proportions and apply Z-score normalization before the Fourier

transform. The graph structure is constructed depending on the distance between sensors following [Guo *et al.*, 2019]. More implementation details are presented in [Appendix E](#).

## 5.4 Experiment Results

Table 2 presents the results of our traffic forecasting experiments, where the prediction task involves forecasting future time series for a 60-minute horizon based on observations from the past 60 minutes. The table includes numerical values for the average RMSE, MAE, and CRPS over the entire forecast window. Additionally, it provides corresponding point evaluations assessed at 15, 30, and 60 minutes such that we can evaluate the short and long-term forecasting performance of the models.

SpecSTG consistently achieves top-tier results across various tasks, demonstrating exceptional performance and competitive forecasting capabilities compared to baseline models. Particularly, its proficiency in deterministic forecasting is evidenced by superior results in terms of RMSE and MAE. In comparison to the second-best model, SpecSTG exhibits an 8.00% improvement in average RMSE for PEMS08S and a 6.24% improvement for PEMS04S. Similarly, the average MAE sees enhancements of 3.55% for PEMS08S and 1.75% for PEMS04F. This superior deterministic performance stems from SpecSTG's unique probabilistic learning process in the spectral domain, leveraging rich global spatial information, which is an acknowledged crucial component in determinis-

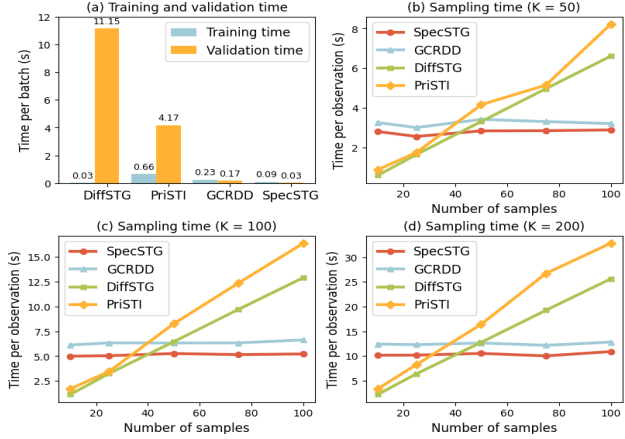


Figure 4: Time efficiency of training, validation, and sampling

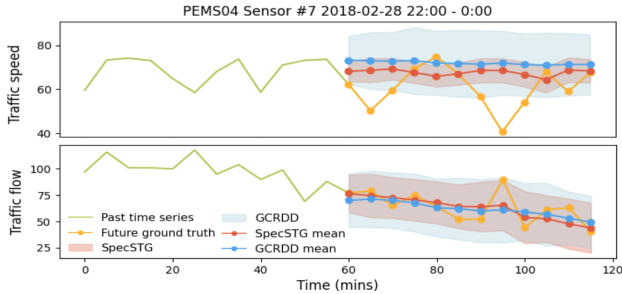


Figure 5: Forecasting visualizations of SpecSTG and GCRDD.

tic traffic forecasting [Yu *et al.*, 2018; Fang *et al.*, 2019]. Regarding CRPS, SpecSTG demonstrates an advantage in traffic flow forecasting compared to vehicle speed forecasting. This is attributed to the higher variations associated with flow data, given that vehicle speed is typically regulated by speed limits. For instance, the standard deviations of data in PEMS08S and PEMS08F are 6.65 and 146.22, respectively. Consequently, the systematic variations measured by the Fourier representation become beneficial in generating a compatible distribution of future traffic flows. We also observe that CSDI and PriSTI excel in predicting traffic flow, leveraging the attention mechanism to process temporal dynamics. On the other hand, TimeGrad and GCRDD exhibit comparably better performance in forecasting vehicle speeds, utilizing a recurrent structure that emphasizes consecutive temporal connectivity. We suppose this distinction is caused by the attention mechanism's effectiveness in capturing global temporal variations and the recurrent structure's aptness for learning highly correlated speed patterns. Our approach, with a recurrent encoder, combines the strengths of both methodologies. It preserves the ability to learn continuous time patterns while enhancing the identification of variations through the incorporation of spectral variation measurements.

## 6 Discussion

In this section, we mainly discuss the time efficiency of SpecSTG and some insights from forecasting visualizations. For more discussions such as comparison with deterministic mod-

els, please refer to Appendices F, G and H.

### 6.1 Time Efficiency

In Figure 4, we compare the training, validation, and sampling time of SpecSTG with three diffusion models for STG forecasting, including GCRDD, DiffSTG, and PriSTI. The training and validation of SpecSTG is clearly faster than GCRDD and PriSTI. But SpecSTG is slightly slower than DiffSTG with training (0.09 s/batch vs. 0.03 s/batch). This deficiency is majorly caused by the non-parallel recurrent encoder, but we perceive this as acceptable given SpecSTG's outstanding performance over DiffSTG. In addition, the validation time of DiffSTG is very long due to its sampling for MAE calculation during validation. To show sampling efficiency, we plot the sampling time per observation (i.e., a future window of 60 minutes) when diffusion steps  $K = 50, 100, 200$ . We set the batch size of one-shot methods, DiffSTG and PriSTI, as 8 and 16, and report the best results. For autoregressive methods, SpecSTG shows a notable time advantage over GCRDD in sampling. Besides, their sampling time does not vary much with the number of samples  $S$ . By contrast, the time cost of one-shot methods increases rapidly with the increase of  $S$ . Although DiffSTG and PriSTI are more efficient when  $S$  is small, a small number of samples often cannot present a clear picture of future data distribution.

### 6.2 Forecasting Visualizations

In Figure 5, we visualize the forecasting outcomes of SpecSTG and GCRDD on PEMS04 sensor #7 in the period from 22:00 to 0:00 on February 28th, 2018. In traffic speed forecasting, SpecSTG's mean estimation is closer to the central tendency of future time series, but the sample distribution of GCRDD better covers the variations of future observations (although some prompt variations are still hard to detect). This matches with the experiment result that SpecSTG has better deterministic results but inferior CRPS. Additionally, in the flow forecasting task, despite SpecSTG and GCRDD obtaining similar results, SpecSTG produces the results with lower variance. This observation also reflects the experiment results that SpecSTG achieves outstanding performance with PEMS04F in terms of all metrics.

## 7 Concluding Remark

In this paper, we proposed SpecSTG, a spectral diffusion approach for fast probabilistic spatio-temporal traffic forecasting. Our method transforms the entire diffusion learning process to the spectral domain by generating the Fourier representation of future time series instead of the original data. Although we have introduced the autoregressive architecture of SpecSTG, the idea of spectral diffusion can be straightforwardly applied to one-shot methods as well by altering the generative target and graph convolution. Hence, SpecSTG can be regarded as an effective framework for STG forecasting. Experiment results confirm the superior performance of SpecSTG, demonstrating more efficient training and inference compared to state-of-the-art diffusion methods. Nevertheless, we highlight that SpecSTG may fall short of predicting compatible future distributions when the data have low variations, diminishing the efficacy of spectral measurements.

## Appendices

### Appendix A. Generalized Fourier Transform

The Fourier transform can be naturally generalized to multivariate traffic STGs. Assume that we have a traffic STG with graph signals  $\mathbf{X}_G = \{\mathbf{x}_1, \mathbf{x}_2, \dots, \mathbf{x}_t, \dots | \mathbf{x}_t \in \mathbb{R}^{N \times D_x}\}$ , where  $D_x$  is the number of variables. The graph is a univariate STG when  $D_x = 1$ , and a multivariate STG when  $D_x \geq 2$ . For a sampled past-future window  $\mathbf{X} = \{\mathbf{x}_{t_0-c+1}, \dots, \mathbf{x}_{t_0+f}\} \in \mathbb{R}^{N \times D_x \times (c+f)}$ , we first split it according to its variables and rewrite it as  $\mathbf{X} = \{\mathbf{x}'_1, \dots, \mathbf{x}'_d, \dots, \mathbf{x}'_{D_x} | \mathbf{x}'_d \in \mathbb{R}^{N \times (c+f)}\}$ . Then, with the Fourier operator  $\mathbf{U}$ , we conduct the transform on each variable matrix  $\mathbf{x}'_d$  as

$$\tilde{\mathbf{x}}'_d = \mathbf{U}^\top \mathbf{x}'_d.$$

Hence, the Fourier representation of the sampled window  $\mathbf{X}$  is  $\tilde{\mathbf{X}} = \{\tilde{\mathbf{x}}'_1, \dots, \tilde{\mathbf{x}}'_d, \dots, \tilde{\mathbf{x}}'_{D_x}\} \in \mathbb{R}^{N \times D_x \times (c+f)}$ . To convert the Fourier representation of a single variable matrix back to the original domain, we may apply Fourier reconstruction as

$$\mathbf{x}'_d = \mathbf{U} \tilde{\mathbf{x}}'_d,$$

so  $\mathbf{X} = \{\mathbf{U} \tilde{\mathbf{x}}'_1, \dots, \mathbf{U} \tilde{\mathbf{x}}'_d, \dots, \mathbf{U} \tilde{\mathbf{x}}'_{D_x}\} \in \mathbb{R}^{N \times D_x \times (c+f)}$ .

### Appendix B. Denoising Diffusion Probabilistic Model

Denoising diffusion probabilistic model (DDPM) is one of the classic formulations of diffusion models [Sohl-Dickstein *et al.*, 2015; Ho *et al.*, 2020; Yang *et al.*, 2023]. With its high flexibility in modelling target distributions and outstanding capability of capturing complex generative patterns, DDPM is widely used in various time series tasks [Rasul *et al.*, 2021a; Tashiro *et al.*, 2021; Coletta *et al.*, 2023; Lin *et al.*, 2023]. Unlike traditional probabilistic models that learn the target distribution  $q(x)$  explicitly to generate samples, DDPM learns how to generate samples directly via a pair of forward-backward Markov chains without accessing the actual target distribution function. Assuming that  $\mathbf{x}^0$  is the original data, for  $k = 0, 1, \dots, K$ , the forward chain injects Gaussian noises to the generative target with a probabilistic transition kernel

$$q(\mathbf{x}^k | \mathbf{x}^{k-1}) = \mathcal{N} \left( \mathbf{x}^k; \sqrt{1 - \beta_k} \mathbf{x}^{k-1}, \beta_k \mathbf{I} \right),$$

where  $\beta_k \in (0, 1)$  is a hyperparameter controlling the noise level at each forward step. The design of forward chain enables us to derive the disturbed data at a particular step  $k$  directly from  $\mathbf{x}^0$  as

$$q(\mathbf{x}^k | \mathbf{x}^0) = \mathcal{N} \left( \mathbf{x}^k; \sqrt{\tilde{\alpha}_k} \mathbf{x}^0, (1 - \tilde{\alpha}_k) \mathbf{I} \right),$$

where  $\tilde{\alpha}_k := \prod_{i=1}^k (1 - \beta_i)$ . This means  $\mathbf{x}^k = \sqrt{\tilde{\alpha}_k} \mathbf{x}^0 + \sqrt{1 - \tilde{\alpha}_k} \mathbf{\epsilon}$  with  $\mathbf{\epsilon} \sim \mathcal{N}(\mathbf{0}, \mathbf{I})$ . To ensure that the forward chain transits eventually to white noises, one shall have  $\tilde{\alpha}_K \approx 0$  such that  $q(\mathbf{x}^K) := \int q(\mathbf{x}^K | \mathbf{x}^0) q(\mathbf{x}^0) d\mathbf{x}^0 \approx \mathcal{N}(\mathbf{x}^K; \mathbf{0}, \mathbf{I})$ . Next, the backward chain recovers white noises to original

data through a Gaussian transition kernel  $p_{\theta}(\mathbf{x}^{k-1} | \mathbf{x}^k) = \mathcal{N}(\mathbf{x}^{k-1}; \mu_{\theta}(\mathbf{x}^k, k), \sigma_k \mathbf{I})$ , where  $\mu_{\theta}(\mathbf{x}^k, k)$  is usually parameterized with a neural network with learnable parameters  $\theta$ , and  $\sigma_k$  is a variance hyperparameter. These parameters are optimized by minimizing the negative evidence lower-bound (ELBO):

$$\mathcal{L}_E(\theta) = \mathbb{E}_{q(\mathbf{x}^0:K)} \left[ -\log p(\mathbf{x}^K) - \sum_{k=1}^K \log \frac{p_{\theta}(\mathbf{x}^{k-1} | \mathbf{x}^k)}{q(\mathbf{x}^k | \mathbf{x}^{k-1})} \right].$$

The learning process is simplified with DDPM by [Ho *et al.*, 2020]. Instead of learning  $\mu_{\theta}(\mathbf{x}^k, k)$ , a denoising network  $\epsilon_{\theta}(\mathbf{x}^k, k)$  is learned with the following objective function:

$$\mathcal{L}_{DDPM}(\theta) = \mathbb{E}_{k, \mathbf{x}^0, \mathbf{\epsilon}} \left\| \mathbf{\epsilon} - \epsilon_{\theta}(\mathbf{x}^k, k) \right\|^2.$$

This denoising network  $\epsilon_{\theta}(\mathbf{x}^k, k)$  takes noised data  $\mathbf{x}^k$  and step index  $k$  as inputs to predict the noise injected at step  $k$  in the forward chain. Finally, DDPM generates samples by eliminating the noises in random white noise  $\mathbf{x}^K \sim \mathcal{N}(\mathbf{x}^K; \mathbf{0}, \mathbf{I})$ . For backward step  $k = K, K-1, \dots, 1$ , DDPM updates the sample as

$$\mathbf{x}^{k-1} \leftarrow \frac{1}{\sqrt{1 - \beta_k}} \left( \mathbf{x}^k - \frac{\beta_k}{\sqrt{1 - \tilde{\alpha}_k}} \epsilon_{\theta}(\mathbf{x}^k, k) \right) + \sigma_k \mathbf{e}$$

where  $\sigma_k$  is a hyperparameter of variance in the backward transition kernel with  $\mathbf{e} = \mathbf{0}$  for  $k = 1$ , and  $\mathbf{e} \sim \mathcal{N}(\mathbf{0}, \mathbf{I})$  otherwise. Eventually,  $\mathbf{x}^0$  will be a sample from the same distribution of the generative target.

### Appendix C. Baselines

In the main experiment, we compare SpecSTG with five state-of-the-art diffusion baselines:

- **TimeGrad** [Rasul *et al.*, 2021a]: an autoregressive diffusion model using long short-term memory (LSTM) or gated recurrent units (GRU) to encode temporal dynamics and a time-modified WaveNet [van den Oord *et al.*, 2016a] as  $\epsilon_{\theta}$ ;
- **CSDI** [Tashiro *et al.*, 2021]: a one-shot diffusion model initially designed for multivariate imputation but with potential in forecasting when masking future time series as missing values. A transformer-based [Vaswani *et al.*, 2017] WaveNet is adopted as its  $\epsilon_{\theta}$ , in which temporal and feature information is processed by two separate transformer layers.
- **GCRDD** [Li *et al.*, 2023]: an autoregressive diffusion model for spatio-temporal forecasting, which adopts a graph-modified GRU to encode past time series and spatial connectivity as conditions. Developed from TimeGrad, GCRDD also employs a WaveNet architecture for its  $\epsilon_{\theta}$  but with graph convolution to process spatial information.
- **DiffSTG** [Wen *et al.*, 2023]: an one-shot diffusion model for spatio-temporal forecasting with graph-modified UNet [Ronneberger *et al.*, 2015] as  $\epsilon_{\theta}$ ;

- **PriSTI** [Liu *et al.*, 2023]: a one-shot diffusion model for spatio-temporal imputation. It is equipped with a feature extraction mechanism to construct conditions. Its  $\epsilon_\theta$  is similar to CSDI but with more specialized attention mechanism to capture spatio-temporal dependencies.

In addition, in **Appendix G**, we provide supplementary comparisons with non-diffusion probabilistic methods, including

- **DeepVAR** [Salinas *et al.*, 2020]: an autoregressive RNN-based model for multivariate time series forecasting, known as the multivariate variant of DeepAR.
- **Transformer Normalizing Flow** [Rasul *et al.*, 2021b]: an autoregressive model for multivariate time series forecasting that approximates the target distribution with a normalizing flow such as Real-NVP [Dinh *et al.*, 2017] and MAF [Papamakarios *et al.*, 2017]. Here we choose Real-NVP, and we call this model TransNVP.
- **MC dropout** [Wu *et al.*, 2021]: a one-shot Bayesian-based model for spatio-temporal uncertainty qualification, implemented with Monte Carlo (MC) dropout [Gal *et al.*, 2017].

Besides, we also consider some classic deterministic methods, including

- **Historical Average (HA)**: a deterministic method that regards time series as periodic processes and predicts future time series with weighted averages from past observations.
- **Vector Auto-Regressive model (VAR)** [Zivot and Wang, 2006]: a deterministic model for multivariate time series forecasting that assumes time series are stationary and predicts with lagged observations.
- **FC-LSTM** [Sutskever *et al.*, 2014]: an LSTM model with fully connected (FC) hidden units that performs well in capturing sequential temporal dependencies.
- **STGCN** [Yu *et al.*, 2018]: a graph convolutional network for spatio-temporal traffic forecasting, equipped with gated temporal convolution and graph convolution to process temporal and spatial information.
- **DCRNN** [Li *et al.*, 2018]: a recurrent graph neural network that integrates graph diffusion and GRU under an encoder-decoder structure.
- **ASTGCN** [Guo *et al.*, 2019]: an attention-based graph convolutional neural network that adopts both graph attention and temporal attention to learn spatio-temporal patterns.
- **GMAN** [Zheng *et al.*, 2020]: a graph neural network with multiple spatio-temporal attention blocks in its encoder-decoder architecture to enhance the learning of spatio-temporal patterns.

## Appendix D. Metrics

We use three metrics to evaluate the performance of SpecSTG, including two deterministic metrics, Root Mean Squared Error (RMSE) and Mean Absolute Error (MAE), and one probabilistic metric, Continuous Ranked Probability Score

(CRPS) . Here, we explain how to calculate these metrics for univariate STG forecasting in our experiments. RMSE and MAE are adopted to measure the distance between predictions and the ground truth. We use the mean of generated samples as predictions to calculate RMSE. In addition, we use the mean and median to compute MAE for all probabilistic methods and report the best results. Given predictions  $\hat{\mathbf{X}}_f$  at time  $t_0$  (after the Fourier reconstruction) and ground truth  $\mathbf{X}_f$  of one future window, the formulas can be written as:

$$\text{RMSE}(\hat{\mathbf{X}}_f, \mathbf{X}_f) = \sqrt{\frac{1}{f} \sum_{t=t_0+1}^{t_0+f} (\mathbf{x}_t - \hat{\mathbf{x}}_t)^2},$$

$$\text{MAE}(\hat{\mathbf{X}}_f, \mathbf{X}_f) = \frac{1}{f} \sum_{t=t_0+1}^{t_0+f} |\mathbf{x}_t - \hat{\mathbf{x}}_t|.$$

The final results reported in our experiments are the averages from all available predictive windows in the test set. CRPS is a probabilistic metric that measures the compatibility of the learned probabilistic distribution at each observation [Matheson and Winkler, 1976]. Given the cumulative distribution function (CDF)  $F$  of the distribution estimated at observation  $x$ , CRPS is defined as

$$\text{CRPS}(F^{-1}, x) = \int_0^1 2(\kappa - \mathbb{I}_{x < F^{-1}(\kappa)})(x - F^{-1}(\kappa)) d\kappa,$$

where  $\kappa \in [0, 1]$ ,  $F^{-1}$  is the quantile function, and  $\mathbb{I}_{x < F^{-1}(\kappa)}$  is an indicator function which equals to 1 when  $x < F^{-1}(\kappa)$  and 0 otherwise. To calculate the integral, we use 100 samples generated at each time point and sensor/node to approximate the corresponding distribution and calculate CRPS following the way defined in [Tashiro *et al.*, 2021]. For each future window, we may compute the normalized CRPS at time point  $t = t_0 + 1, \dots, t_0 + f$  as

$$\frac{\sum_n \text{CRPS}(F_{t,n}^{-1}, x_{t,n})}{\sum_n |x_{t,n}|},$$

where  $n = 1, \dots, N$  denotes each sensor/node, and  $x_{t,n}$  is the value of sensor/node  $n$  at time  $t$ . Likewise, the “CRPS Avg.” is computed as

$$\frac{\sum_{t,n} \text{CRPS}(F_{t,n}^{-1}, x_{t,n})}{\sum_{t,n} |x_{t,n}|}.$$

We do not adopt  $\text{CRPS}_{sum}$  [Rasul *et al.*, 2021a; Tashiro *et al.*, 2021] as a metric because sensors are not regarded as features in our experiments. The results reported for CRPS are also averages over all available predictive windows in the test set.

## Appendix E. Implementation Details

Here we provide supplementary implementation details of SpecSTG and baseline models.

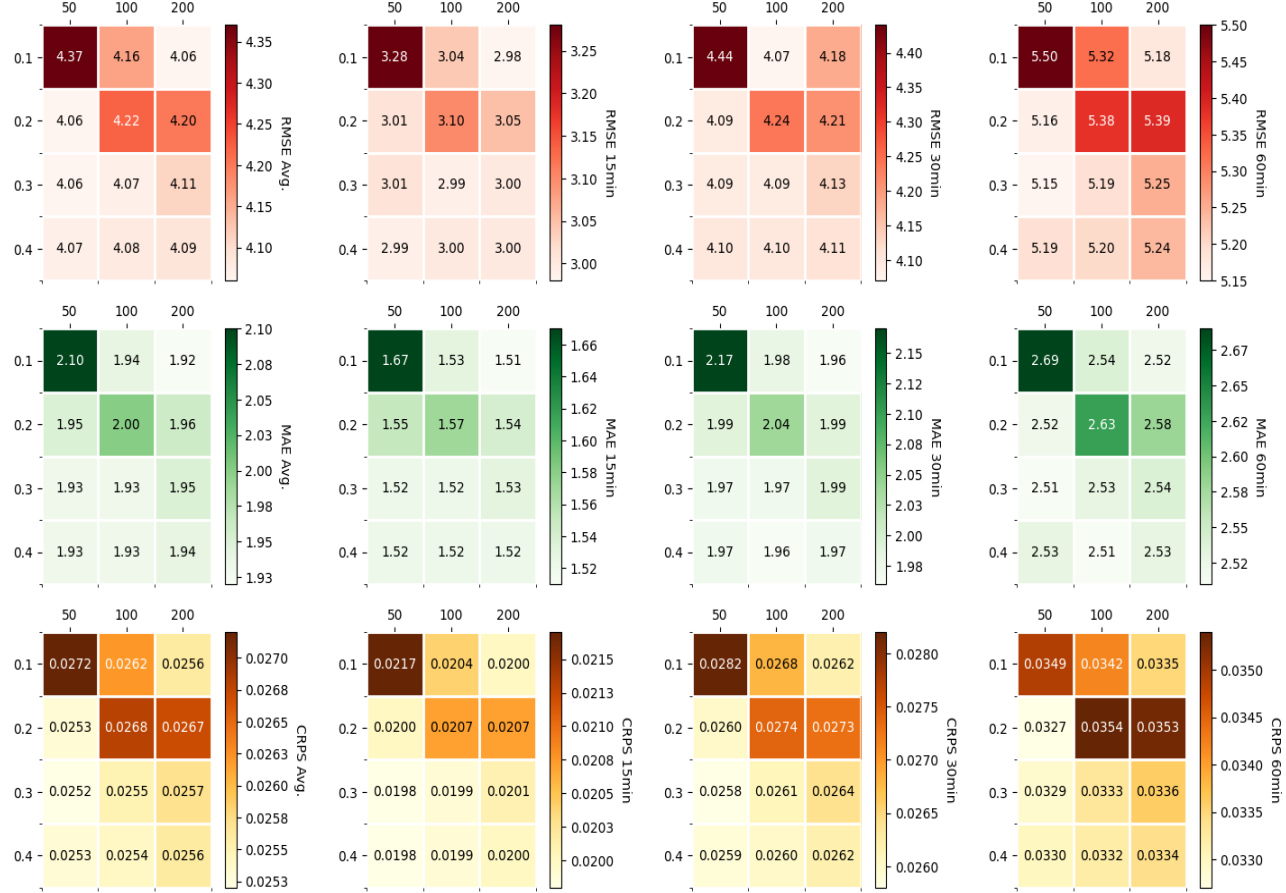


Figure 6: Hyperparameter study on the end of variance schedule  $\beta_K$ , and the number of diffusion steps  $K$ , with PEMS04S. The changes in average RMSE, MAE, CRPS, and their point values at 15/30/60 minutes are shown with heatmaps. Lower values indicate better forecasting performance.

**Training:** Each training epoch contains 200 training batches and 50 validation batches randomly selected from training and validation sets. The batch size for baseline models is selected from [8, 16, 32, 64]. For SpecSTG, the dropout rate and the weight decay parameter in  $\ell_2$ -regularization are set to 0.1 and  $1e-6$ , respectively. We also apply dropout and  $\ell_2$ -regularization to baseline models with the default settings from their original papers. Moreover, hyperparameter tuning is conducted with random search when needed.

**Diffusion baselines:** Diffusion models are implemented with similar diffusion process hyperparameters as SpecSTG. For all models that utilize WaveNet architecture in their denoising networks, we fix the number of residual blocks and residual channels both as 8. Other model-specific implementation details follow their original papers along with the default settings in their codes.

**Non-diffusion probabilistic baselines:** DeepVAR is implemented with PyTorchTS from <https://github.com/zalandoresearch/pytorch-ts>. We choose the LSTM with 2 layers as its recurrent structure. The size of hidden states is fixed at 1024, because a smaller hidden size leads to unsatisfactory performance, and a larger hidden size will not im-

prove the results much. TransNVP is also implemented with PyTorchTS. Given that details of TransNVP are not mentioned in its paper, we set its hyperparameters majorly according to the settings of Transformer MAF, which is a similar model but uses MAF to model the target distribution. We also tune the hyperparameters when needed to improve the performance of TransNVP. Lastly, the implementation of MC Dropout follows its original paper and codes.

**Deterministic baselines:** The results of deterministic baselines are retrieved directly from the experiments in [Shao *et al.*, 2022], which adopts similar experiment settings (e.g., 60%/20%/20% data split) as our experiments.

## Appendix F. Hyperparameter Study

In the hyperparameter study, we focus on the combination of two very important diffusion hyperparameters: the number of diffusion steps,  $K$ , and the end of noise schedule,  $\beta_K$ . Theoretically, the choices of  $K$  and  $\beta_K$  are relevant to each other. Since the noise level gradually increases from  $\beta_1 = 1e-4$  to  $\beta_K$  in  $K$  diffusion steps, these two hyperparameters control the changing speed and level of noises in the diffusion process, which is essential for the white noise assumption of

Model	RMSE				MAE				CRPS			
	Avg.	15min	30min	60min	Avg.	15min	30min	60min	Avg.	15min	30min	60min
PEMS04F												
DeepVAR	50.59	43.90	48.76	60.46	37.74	32.97	36.72	45.87	0.2094	0.1997	0.2108	0.2209
TransNVP	82.74	68.26	81.7	99.81	61.85	53.06	62.25	73.49	0.2359	0.2008	0.2377	0.2819
MC dropout	<u>33.52</u>	<u>30.62</u>	<u>33.23</u>	<u>37.84</u>	<u>21.77</u>	<u>19.59</u>	<u>21.58</u>	<u>25.28</u>	<u>0.0847</u>	<u>0.0771</u>	<u>0.0843</u>	<u>0.0969</u>
SpecDiff	<b>33.15</b>	<b>30.17</b>	<b>32.81</b>	<b>37.29</b>	<b>21.53</b>	<b>19.29</b>	<b>21.39</b>	<b>23.29</b>	<b>0.0766</b>	<b>0.0689</b>	<b>0.0761</b>	<b>0.0886</b>
PEMS08F												
DeepVAR	41.43	35.83	39.88	49.41	27.86	23.19	27.03	34.89	0.1291	0.1219	0.1269	0.1412
TransNVP	67.69	60.48	68.48	76.16	51.37	49.08	52.31	58.38	0.1802	0.1601	0.1822	0.2073
MC dropout	<u>25.74</u>	<u>23.16</u>	<u>25.55</u>	<b>29.47</b>	<b>16.85</b>	<u>15.23</u>	<u>16.71</u>	<b>19.56</b>	<u>0.0681</u>	<u>0.0617</u>	<u>0.0676</u>	<u>0.0788</u>
SpecDiff	<b>25.59</b>	<b>22.23</b>	<b>24.77</b>	<u>29.90</u>	<u>17.06</u>	<b>14.93</b>	<b>16.70</b>	<u>20.25</u>	<b>0.0572</b>	<b>0.0500</b>	<b>0.0558</b>	<b>0.0680</b>
PEMS04S												
DeepVAR	6.23	5.72	6.11	6.93	2.76	2.52	2.72	3.13	0.0490	0.0450	0.0488	0.0549
TransNVP	6.25	5.73	6.27	6.98	3.36	3.12	3.39	3.74	0.0408	0.0382	0.0412	0.0446
MC dropout	<u>4.22</u>	<b>2.99</b>	<u>4.17</u>	<u>5.50</u>	<b>1.83</b>	<b>1.41</b>	<b>1.85</b>	<b>2.45</b>	<u>0.0261</u>	<u>0.0201</u>	<u>0.0264</u>	<u>0.0350</u>
SpecDiff	<b>4.06</b>	<u>3.01</u>	<b>4.09</b>	<u>5.15</u>	1.93	<u>1.52</u>	<u>1.97</u>	<u>2.51</u>	<b>0.0252</b>	<b>0.0198</b>	<b>0.0258</b>	<b>0.0329</b>
PEMS08S												
DeepVAR	5.73	5.55	5.7	6.05	2.56	2.42	2.57	2.79	0.0544	0.0534	0.0543	0.0558
TransNVP	5.41	5.12	5.54	5.74	2.76	2.64	2.83	2.91	0.0349	0.0334	0.0358	0.0368
MC dropout	<u>3.57</u>	2.59	<u>3.55</u>	<u>4.62</u>	<b>1.52</b>	<b>1.19</b>	<b>1.54</b>	<b>2.01</b>	<u>0.0229</u>	<u>0.0179</u>	<u>0.0232</u>	<u>0.0302</u>
SpecDiff	<b>3.45</b>	<b>2.58</b>	<b>3.46</b>	<b>4.36</b>	<u>1.63</u>	<u>1.27</u>	<u>1.67</u>	<u>2.12</u>	<b>0.0217</b>	<b>0.0170</b>	<b>0.0219</b>	<b>0.0286</b>

Table 5: Comparison between SpecSTG and non-diffusion probabilistic models in traffic flow and speed forecasting tasks. The best results are marked in **bold**, and the second best results are underlined.

diffusion models.

The same as the implementation of SpecSTG in our experiments, we set the search spaces of  $\beta_K$  and  $K$  as  $[0.1, 0.2, 0.3, 0.4]$  and  $[50, 100, 200]$ , respectively. In Figure 6, we use heatmaps to show the change in model performance in terms of RMSE, MAE, and CRPS on PEMS04S with different hyperparameter combinations. We observe that SpecSTG typically performs better with a larger  $\beta_K$  (for instance 0.3 or 0.4). The best results appear when  $\beta_K = 0.3$  and  $K = 50$ . It is also worth noting that the forecasting performance of SpecSTG does not vary dramatically with different hyperparameter combinations. This means our method is not very sensitive to hyperparameter selection, alleviating the burden of hyperparameter tuning.

## Appendix G. Supplementary Comparisons

In Section 5, we have compared SpecSTG with state-of-the-art diffusion approaches on PEMS04 and PEMS08 in traffic flow and speed forecasting tasks. Now, we provide more comparisons between SpecSTG and other methods. More specifically, we introduce more baseline models including three non-diffusion probabilistic models and seven classic deterministic models.

In Table 5, we exhibit the results of the comparison between SpecSTG and three non-diffusion methods. Overall, SpecSTG attains the best results for most metrics and tasks, and presents a clear advantage in producing compatible distributions of future time series. DeepVAR and TransNVP, which are initially designed for traditional multivariate time series forecasting, fail to achieve promising results in traffic forecasting tasks. On the contrary, MC dropout is a competitive baseline model, especially regarding MAE. We suppose this is attributed to its MAE-based objective function, which

Model	RMSE			MAE		
	15min	30min	60min	15min	30min	60min
PEMS04F						
HA	42.69	49.37	67.43	28.92	33.73	46.97
VAR	34.30	36.58	40.28	21.94	23.72	26.76
FC-LSTM	33.37	39.1	50.73	21.42	25.83	36.41
STGCN	30.76	34.43	41.11	19.35	21.85	26.97
DCRNN	31.94	36.15	44.81	20.34	23.21	29.24
ASTGCN	31.43	34.34	40.02	20.15	22.09	26.03
GMAN	<b>29.32</b>	<b>30.77</b>	<b>30.21</b>	<b>18.28</b>	<b>18.75</b>	<b>19.95</b>
SpecSTG	<u>30.17</u>	<u>32.81</u>	<u>37.29</u>	<u>19.29</u>	<u>21.39</u>	<u>23.29</u>
PEMS08F						
HA	34.96	40.89	56.74	23.52	27.67	39.28
VAR	29.73	30.30	38.97	19.52	22.25	26.17
FC-LSTM	26.27	34.53	47.03	17.38	21.22	30.69
STGCN	25.03	27.27	34.21	15.30	17.69	25.46
DCRNN	25.48	27.63	34.21	15.64	17.88	22.51
ASTGCN	25.09	28.17	33.68	16.48	18.66	22.83
GMAN	22.88	<b>24.02</b>	<b>25.96</b>	<b>13.80</b>	<b>14.62</b>	<b>15.72</b>
SpecSTG	<b>22.23</b>	<u>24.77</u>	<u>29.90</u>	<u>14.93</u>	<u>16.70</u>	<u>20.25</u>

Table 6: Comparison between SpecSTG and classic deterministic models on PEMS04F and PEMS08F. Partial results are retrieved from [Shao *et al.*, 2022]. The best results are marked in **bold**, and the second best results are underlined.

guides the model to generate better MAE results during the training process, and better test MAE eventually.

Table 6 presents a comparison between SpecSTG and deterministic methods. Notably, SpecSTG outperforms most classic deterministic approaches, including traditional statistical models like VAR and graph neural networks such as DCRNN and ASTGCN. However, GMAN consistently demonstrates superior performance, particularly in long-term forecasting. Here are two plausible explanations. Firstly, being a deterministic model, GMAN is trained with MAE loss, strengthening the generation of accurate deterministic pre-

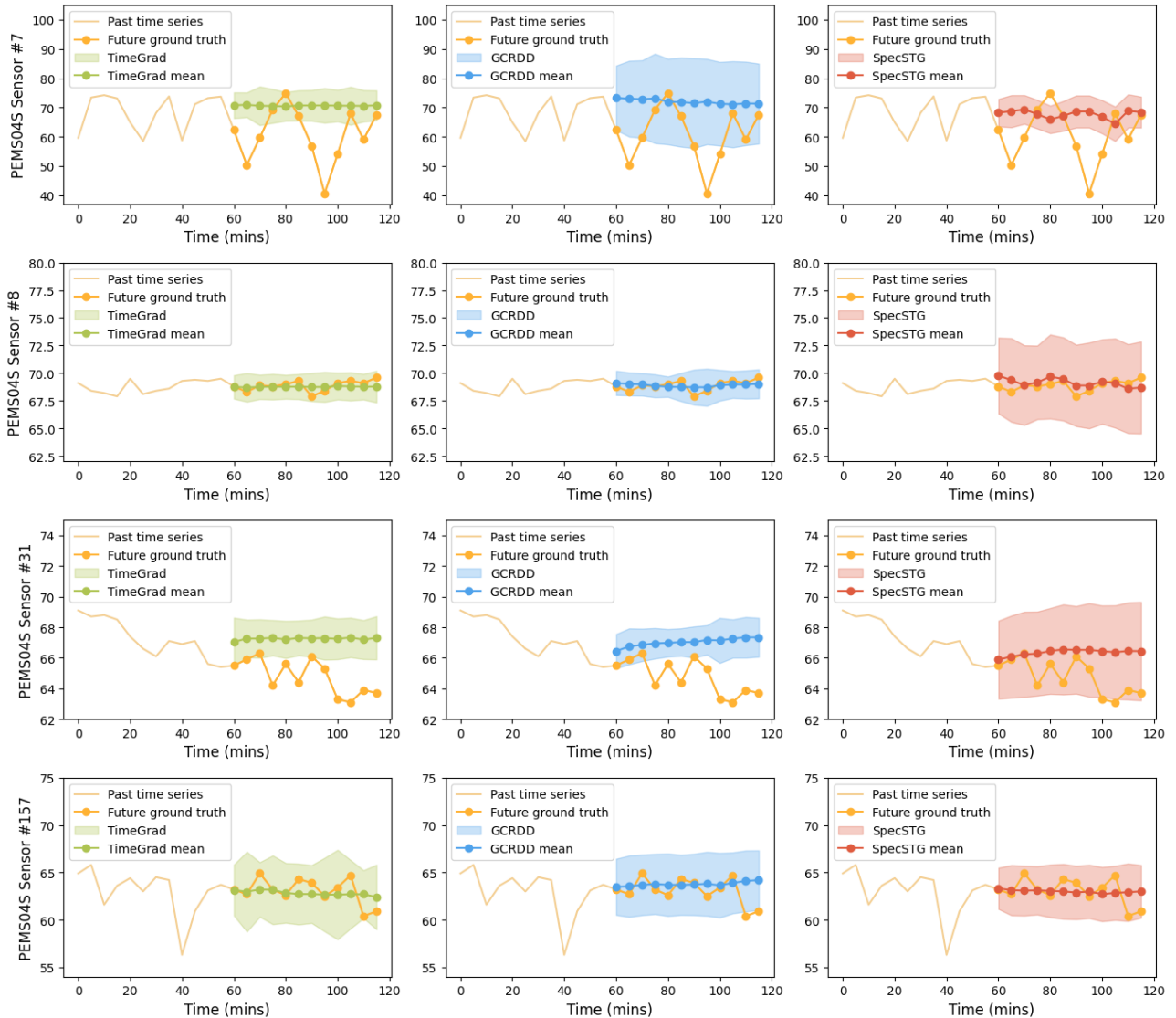


Figure 7: Forecasting visualizations of TimeGrad, GCRDD, and SpecSTG on PEMS04S. SpecSTG provides more accurate deterministic predictions but may fail to generate compatible future distributions in some cases.

dictions compared to SpecSTG, which optimizes an implicit probabilistic objective. Secondly, GMAN’s sophisticated encoder-decoder architecture and multiple spatio-temporal attention blocks effectively integrate spatial and temporal information, while SpecSTG relies on a single graph-modified GRU encoder for processing spatio-temporal patterns. This observation could guide future work to enhance our model.

## Appendix H. Forecasting visualizations

Additional forecasting visualizations for PEMS04S and PEMS04F are presented in Figure 7 and Figure 8, respectively. These figures display the mean and 95% confidence interval of estimated distributions from TimeGrad, GCRDD, and SpecSTG, plotted at the same sensors for comparison.

As discussed in Section 6.2, the low global variation in PEMS04S may reduce the effectiveness of SpecSTG in learning compatible future distributions. Upon closer examination of the data patterns, we observe that this impact is particularly pronounced in windows with very large or very small variations (e.g., sensor #7 and #8). In contrast, distributions estimated by SpecSTG at sensors with moderate variations (e.g., sensor #31 and #157) exhibit a better ability to capture future uncertainty compared to TimeGrad and GCRDD. On PEMS04F, a dataset characterized by high systematic variation, SpecSTG demonstrates promising performance by generating both more accurate deterministic predictions and more compatible distributions.

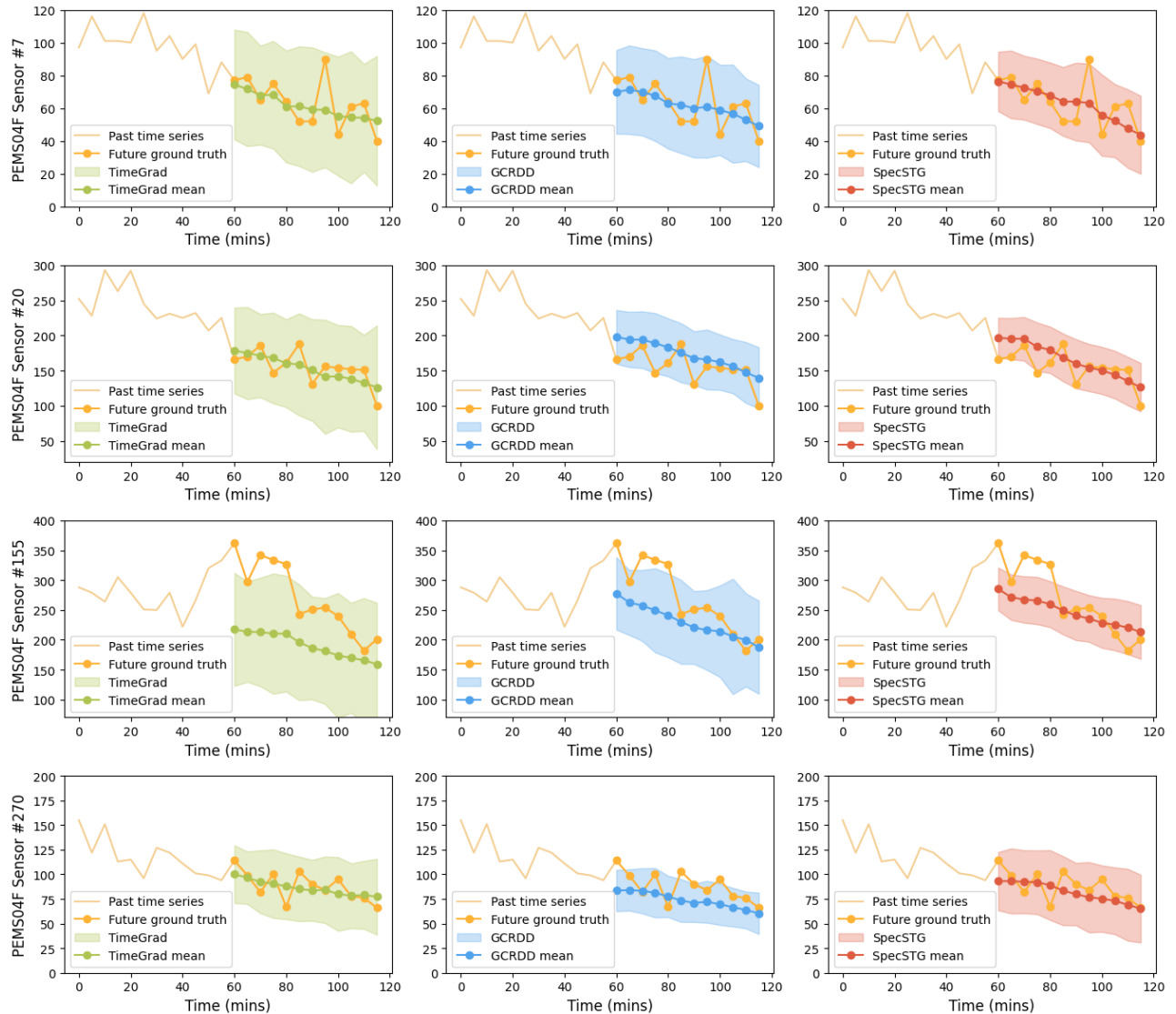


Figure 8: Forecasting visualizations of TimeGrad, GCRDD, and SpecSTG on PEMS04F. SpecSTG produces better deterministic predictions and more compatible distributions than TimeGrad and GCRDD.

## References

[Boukerche *et al.*, 2020] Azzedine Boukerche, Yanjie Tao, and Peng Sun. Artificial intelligence-based vehicular traffic flow prediction methods for supporting intelligent transportation systems. *Computer Networks*, 182:107484, 2020.

[Chen *et al.*, 2001] Chao Chen, Karl Petty, Alexander Skabardonis, Pravin Varaiya, and Zhanfeng Jia. Freeway performance measurement system: mining loop detector data. *Transportation Research Record*, 1748(1):96–102, 2001.

[Chung, 1997] Fan RK Chung. *Spectral graph theory*, volume 92. American Mathematical Society, 1997.

[Coletta *et al.*, 2023] A. Coletta, S. Gopalakrishnan, D. Borrajo, and S. Vyettrenko. On the constrained time-series generation problem. *arXiv preprint*, 2307.01717, 2023.

[Croitoru *et al.*, 2023] Florinel-Alin Croitoru, Vlad Hondru, Radu Tudor Ionescu, and Mubarak Shah. Diffusion models in vision: A survey. *IEEE Transactions on Pattern Analysis and Machine Intelligence*, to appear, 2023.

[Defferrard *et al.*, 2016] Michaël Defferrard, Xavier Bresson, and Pierre Vandergheynst. Convolutional neural networks on graphs with fast localized spectral filtering. In *Advances in Neural Information Processing Systems (NeurIPS)*, volume 29, 2016.

[Dinh *et al.*, 2017] Laurent Dinh, Jascha Sohl-Dickstein, and Samy Bengio. Density estimation using real NVP. In *International Conference on Learning Representations (ICLR)*, 2017.

[Fan *et al.*, 2023] Wenqi Fan, Chengyi Liu, Yunqing Liu, Jiatong Li, Hang Li, Hui Liu, Jiliang Tang, and Qing Li.

Generative diffusion models on graphs: Methods and applications. *International Joint Conference on Artificial Intelligence (IJCAI)*, 2023.

[Fang *et al.*, 2019] Shen Fang, Qi Zhang, Gaofeng Meng, Shiming Xiang, and Chunhong Pan. Gstnet: Global spatial-temporal network for traffic flow prediction. In *International Joint Conference on Artificial Intelligence (IJCAI)*, pages 2286–2293, 2019.

[Gal *et al.*, 2017] Yarin Gal, Jiri Hron, and Alex Kendall. Concrete dropout. *Advances in Neural Information Processing Systems (NeurIPS)*, 30, 2017.

[Guo *et al.*, 2019] Shengnan Guo, Youfang Lin, Ning Feng, Chao Song, and Huaiyu Wan. Attention based spatial-temporal graph convolutional networks for traffic flow forecasting. In *Proceedings of the AAAI Conference on Artificial Intelligence*, volume 33, pages 922–929, 2019.

[Ho *et al.*, 2020] Jonathan Ho, Ajay Jain, and Pieter Abbeel. Denoising diffusion probabilistic models. In *Advances in Neural Information Processing Systems (NeurIPS)*, volume 33, pages 6840–6851, 2020.

[Hu *et al.*, 2023] Junfeng Hu, Xu Liu, Zhencheng Fan, Yuxuan Liang, and Roger Zimmermann. Towards unifying diffusion models for probabilistic spatio-temporal graph learning. *arXiv:2310.17360*, 2023.

[Jin *et al.*, 2023a] Guangyin Jin, Yuxuan Liang, Yuchen Fang, Zezhi Shao, Jincai Huang, Junbo Zhang, and Yu Zheng. Spatio-temporal graph neural networks for predictive learning in urban computing: A survey. *IEEE Transactions on Knowledge and Data Engineering*, 2023.

[Jin *et al.*, 2023b] Ming Jin, Huan Yee Koh, Qingsong Wen, Daniele Zambon, Cesare Alippi, Geoffrey I Webb, Irwin King, and Shirui Pan. A survey on graph neural networks for time series: Forecasting, classification, imputation, and anomaly detection. *arXiv:2307.03759*, 2023.

[Kipf and Welling, 2016] Thomas N. Kipf and Max Welling. Semi-supervised classification with graph convolutional networks. In *International Conference on Learning Representations (ICLR)*, 2016.

[Kong *et al.*, 2021] Zhifeng Kong, Wei Ping, Jiaji Huang, Kexin Zhao, and Bryan Catanzaro. DiffWave: A versatile diffusion model for audio synthesis. In *International Conference on Learning Representations (ICLR)*, pages 1–8, 2021.

[Kreuzer *et al.*, 2021] Devin Kreuzer, Dominique Beaini, Will Hamilton, Vincent Létourneau, and Prudencio Tossou. Rethinking graph transformers with spectral attention. In *Advances in Neural Information Processing Systems (NeurIPS)*, volume 34, pages 21618–21629, 2021.

[Lana *et al.*, 2018] Ibai Lana, Javier Del Ser, Manuel Velez, and Eleni I Vlahogianni. Road traffic forecasting: Recent advances and new challenges. *IEEE Intelligent Transportation Systems Magazine*, 10(2):93–109, 2018.

[Li *et al.*, 2018] Yaguang Li, Rose Yu, Cyrus Shahabi, and Yan Liu. Diffusion convolutional recurrent neural network: Data-driven traffic forecasting. In *International Conference on Learning Representations (ICLR)*, pages 1–8, 2018.

[Li *et al.*, 2023] Ruikun Li, Xuliang Li, Shiying Gao, ST Boris Choy, and Junbin Gao. Graph convolution recurrent denoising diffusion model for multivariate probabilistic temporal forecasting. In *International Conference on Advanced Data Mining and Applications (ADMA)*, pages 661–676. Springer, 2023.

[Liang *et al.*, 2023] Guojun Liang, Prayag Tiwari, Sławomir Nowaczyk, Stefan Byttner, and Fernando Alonso-Fernandez. Dynamic causal explanation based diffusion-variational graph neural network for spatio-temporal forecasting. *arXiv:2305.09703*, 2023.

[Lin *et al.*, 2023] Lequan Lin, Zhengkun Li, Ruikun Li, Xuliang Li, and Junbin Gao. Diffusion models for time-series applications: a survey. *Frontiers of Information Technology and Electronic Engineering*, pages 1–23, 2023.

[Liu *et al.*, 2023] Mingzhe Liu, Han Huang, Hao Feng, Leilei Sun, Bowen Du, and Yanjie Fu. PriSTI: A conditional diffusion framework for spatiotemporal imputation. In *International Conference on Data Engineering (ICDE)*, pages 1–10, 2023.

[Luo *et al.*, 2023] Tianze Luo, Zhanfeng Mo, and Sinno Jialin Pan. Fast graph generation via spectral diffusion. *IEEE Transactions on Pattern Analysis and Machine Intelligence*, 2023.

[Matheson and Winkler, 1976] James E Matheson and Robert L Winkler. Scoring rules for continuous probability distributions. *Management Science*, 22(10):1087–1096, 1976.

[Pal *et al.*, 2021] Soumyasundar Pal, Liheng Ma, Yingxue Zhang, and Mark Coates. Rnn with particle flow for probabilistic spatio-temporal forecasting. In *International Conference on Machine Learning (ICML)*, pages 8336–8348. PMLR, 2021.

[Papamakarios *et al.*, 2017] George Papamakarios, Theo Pavlakou, and Iain Murray. Masked autoregressive flow for density estimation. *Advances in Neural Information Processing Systems (NeurIPS)*, 30, 2017.

[Rasul *et al.*, 2021a] Kashif Rasul, Calvin Seward, Ingmar Schuster, and Roland Vollgraf. Autoregressive denoising diffusion models for multivariate probabilistic time series forecasting. In *International Conference on Machine Learning (ICML)*, pages 8857–8868, 2021.

[Rasul *et al.*, 2021b] Kashif Rasul, Abdul-Saboor Sheikh, Ingmar Schuster, Urs Bergmann, and Roland Vollgraf. Multi-variate probabilistic time series forecasting via conditioned normalizing flows. In *International Conference on Learning Representations*, pages 1–8, 2021.

[Ronneberger *et al.*, 2015] Olaf Ronneberger, Philipp Fischer, and Thomas Brox. U-net: Convolutional networks for biomedical image segmentation. In *Medical Image Computing and Computer-Assisted Intervention*, pages 234–241. Springer, 2015.

[Salinas *et al.*, 2020] David Salinas, Valentin Flunkert, Jan Gasthaus, and Tim Januschowski. Deepar: Probabilistic forecasting with autoregressive recurrent networks. *International Journal of Forecasting*, 36(3):1181–1191, 2020.

[Seo *et al.*, 2018] Youngjoo Seo, Michaël Defferrard, Pierre Vandergheynst, and Xavier Bresson. Structured sequence modeling with graph convolutional recurrent networks. In *International Conference on Neural Information Processing (ICONIP)*, pages 362–373. Springer, 2018.

[Shao *et al.*, 2022] Zezhi Shao, Zhao Zhang, Wei Wei, Fei Wang, Yongjun Xu, Xin Cao, and Christian S. Jensen. Decoupled dynamic spatial-temporal graph neural network for traffic forecasting. *Proceedings of the VLDB Endowment*, 15(11):2733–2746, 2022.

[Sohl-Dickstein *et al.*, 2015] Jascha Sohl-Dickstein, Eric Weiss, Niru Maheswaranathan, and Surya Ganguli. Deep unsupervised learning using nonequilibrium thermodynamics. In *International Conference on Machine Learning (ICML)*, pages 2256–2265. PMLR, 2015.

[Sutskever *et al.*, 2014] Ilya Sutskever, Oriol Vinyals, and Quoc V Le. Sequence to sequence learning with neural networks. *Advances in Neural Information Processing Systems (NeurIPS)*, 27, 2014.

[Tashiro *et al.*, 2021] Yusuke Tashiro, Jiaming Song, Yang Song, and Stefano Ermon. CSDI: Conditional score-based diffusion models for probabilistic time series imputation. In *Advances in Neural Information Processing Systems (NeurIPS)*, volume 34, pages 24804–24816, 2021.

[van den Oord *et al.*, 2016a] Aäron van den Oord, Sander Dieleman, Heiga Zen, Karen Simonyan, Oriol Vinyals, Alex Graves, Nal Kalchbrenner, Andrew W. Senior, and Koray Kavukcuoglu. WaveNet: A generative model for raw audio. In *The 9th ISCA Speech Synthesis Workshop*, page 125, 2016.

[Van den Oord *et al.*, 2016b] Aaron Van den Oord, Nal Kalchbrenner, Lasse Espeholt, Oriol Vinyals, Alex Graves, and Koray Kavukcuoglu. Conditional image generation with PixelCNN decoders. In *Advances in Neural Information Processing Systems (NeurIPS)*, volume 29, 2016.

[Vaswani *et al.*, 2017] Ashish Vaswani, Noam Shazeer, Niki Parmar, Jakob Uszkoreit, Llion Jones, Aidan N Gomez, Łukasz Kaiser, and Illia Polosukhin. Attention is all you need. In *Advances in Neural Information Processing Systems (NeurIPS)*, volume 30, pages 6000–6010, 2017.

[Wen *et al.*, 2023] Haomin Wen, Youfang Lin, Yutong Xia, Huaiyu Wan, Qingsong Wen, Roger Zimmermann, and Yuxuan Liang. DiffSTG: Probabilistic spatio-temporal graph forecasting with denoising diffusion models. In *ACM International Conference on Advances in Geographic Information Systems (ACM SIGSPATIAL)*, pages 1–12, 2023.

[Wu *et al.*, 2021] Dongxia Wu, Liyao Gao, Matteo Chinazzi, Xinyue Xiong, Alessandro Vespignani, Yi-An Ma, and Rose Yu. Quantifying uncertainty in deep spatiotemporal forecasting. In *Proceedings of ACM SIGKDD Conference on Knowledge Discovery & Data Mining (KDD)*, pages 1841–1851, 2021.

[Yang *et al.*, 2023] Ling Yang, Zhilong Zhang, Yang Song, Shenda Hong, Runsheng Xu, Yue Zhao, Wentao Zhang, Bin Cui, and Ming-Hsuan Yang. Diffusion models: A comprehensive survey of methods and applications. *ACM Computing Surveys*, 56(4):1–39, 2023.

[Yu *et al.*, 2018] Bing Yu, Haoteng Yin, and Zhanxing Zhu. Spatio-temporal graph convolutional networks: A deep learning framework for traffic forecasting. *International Joint Conference on Artificial Intelligence (IJCAI)*, 2018.

[Yuan and Li, 2021] Haitao Yuan and Guoliang Li. A survey of traffic prediction: from spatio-temporal data to intelligent transportation. *Data Science and Engineering*, 6:63–85, 2021.

[Zheng *et al.*, 2020] Chuanpan Zheng, Xiaoliang Fan, Cheng Wang, and Jianzhong Qi. Gman: A graph multi-attention network for traffic prediction. In *Proceedings of the AAAI Conference on Artificial Intelligence*, volume 34, pages 1234–1241, 2020.

[Zivot and Wang, 2006] Eric Zivot and Jiahui Wang. Vector autoregressive models for multivariate time series. *Modeling Financial Time Series with S-PLUS®*, pages 385–429, 2006.